Sens Imaging
DOI 10.1007/s11220-013-0079-z

ORIGINAL PAPER

Design of an Orthodontic Torque Simulator for Measurement of Bracket Deformation

G. W. Melenka · D. S. Nobes · P. W. Major · J. P. Carey

Received: 21 August 2012

Abstract The design and testing of an orthodontic torque simulator that reproduces the effect of archwire rotation on orthodontic brackets is described. This unique device is capable of simultaneously measuring the deformation and loads applied to an orthodontic bracket due to archwire rotation. Archwire rotation is used by orthodontists to correct the inclination of teeth within the mouth. This orthodontic torque simulator will provide knowledge of the deformation and loads applied to orthodontic bracket that will aide clinicians by describing the effect of archwire rotation on brackets. This will also impact that design on new archwire\bracket systems by providing an assessment of performance. Deformation of the orthodontic bracket tie wings is measured using a digital image correlation process to measure elastic and plastic deformation. The magnitude of force and moments applied to the bracket though the archwire is also measured using a six-axis load cell. Initial tests have been performed on two orthodontic brackets of varying geometry to demonstrate the measurement capability of the orthodontic torque simulator. The demonstration experiment shows that a Damon Q bracket had a final plastic deformation after a single loading of 0.022 mm while the Speed bracket deformed 0.071 mm. This indicates that the Speed bracket plastically deforms 3.2 times more than the Damon Q bracket for similar magnitude of applied moment. The demonstration experiment demonstrates that bracket geometry affect the deformation of orthodontic brackets and this difference can be detected using the orthodontic torque simulator.

G. W. Melenka · D. S. Nobes · J. P. Carey (✉)
Mechanical Engineering, Faculty of Engineering, University of Alberta, Edmonton, AB T6G 2G8, Canada
e-mail: jpcarey@ualberta.ca

P. W. Major
Department of Dentistry, Faculty of Medicine and Dentistry, University of Alberta, Edmonton, AB T6G 2N8, Canada

Published online: 01 August 2013

Keywords Orthodontic bracket · Deformation · Contact-free optical displacement measurement · Digital image correlation

1 Introduction

Braces and archwires are used by orthodontists to correct teeth misalignment (malocclusions) within the dental arch [1]. Braces are typically worn for over 2 years and patients require regular checkups to monitor and adjust the realignment progress [2]. Braces consist of a series of brackets that are bonded to the crown of individual teeth and an archwire which passes between each and is ligated to the brackets. Tooth motion for re-alignment is achieved by applying forces and moments to the crown of the tooth through the interaction archwire with the bracket. Short term tooth movement results from the stimulation of the periodontal ligament (PDL), the connective tissue which attaches the tooth to the alveolar bone [1, 3]. Forces applied through the tooth's crown apply pressure and cause deformation of the PDL. Pressures applied to the PDL are alleviated initially by creep-like internal fluid flow, which is then followed by the resorption and apposition of alveolar bone to support the tooth in its post-loading position [1, 3]. Tooth movement is therefore the result of the mechanical interaction of the archwire with the bracket. The orthodontic definition of "torque" refers to the angle of rotation of an archwire within a bracket slot and is used to control the inclination of a tooth in the dental arch [12].

Several studies have examined archwire rotation in a bracket to investigate bracket deformation and if permanent distortion of the bracket is possible [4–8]. These studies have measured brackets before and after an applied archwire rotation and investigation of the changes in the shape of the brackets have been used to determine if permanent deformation of the bracket is present. Several of these studies have made reference to bracket deformation but the deformation was not quantified [4, 5, 7]. One study measured the permanent change in titanium and stainless steel bracket slot profile before and after archwire rotation using a stereomicroscope to quantify bracket deformation [6]. This study was limited to only measuring permanent change to the bracket slot and an assessment of the measurement resolution was not given. The findings from this study indicate that plastic deformation occurs to orthodontic brackets due to a 45° archwire rotation. Similarly, another study measured bracket deformation at a variety of archwire rotation angles [8]. Bracket deformation was measured optically using a stereomicroscope and a protractor with a reported resolution of 0.2°. These studies are limited since they are unable to determine the applied moment where permanent deformation begins to occur.

The effect of incremental archwire twist on the loads experienced by orthodontic brackets has also been examined [9–11] by measuring the bulk forces and moments applied to the bracket by an archwire using load cells connected to the bracket. These approaches are limited in that it is unresolved whether the bracket under goes elastic and plastic deformation, what the interaction mechanism is between the archwire and the bracket, and what properties of the mechanical coupling are

important. These unresolved questions complicate the development of a model which would be used to optimize the mechanical system.

The small size, complicated geometries, and complex loading conditions of orthodontic brackets means that most conventional measurement methods are impractical. To investigate the deformation of a bracket as an archwire is rotated within the bracket slot an optical method has been developed, designed, and constructed at the University of Alberta through a collaboration between the Department of Mechanical Engineering and Department of Dentistry. This has been coupled to an existing torque measurement device used to measure the forces and moments applied to brackets [9]. A CCD camera and a full-field digital image correlation (DIC) measurement based system was added to this device in order to measure the displacement of bracket tie wings [12]. This device has also been used to demonstrate the deformation of self-ligating brackets and to compare geometrically similar titanium and stainless steel brackets [13, 14]. The testing apparatus comprises of a 6-axis load cell which measures forces and moments applied to a test bracket and using the DIC-based imaging system to measures displacement/bracket-archwire interaction. This device allows for the simulation of the rotation of an archwire within a bracket slot and can be used to measure the deformation that occurs to these brackets which can be correlated to applied loads. Understanding the loads that are applied to orthodontic brackets and the deformation of the brackets is required to improve treatment efficiency and to generate models of the interaction of bracket-archwire-tooth for system optimization. Therefore, the deformation of orthodontic brackets should be measured for varying archwire angulations, bracket geometries, archwire size and ligation method in order to provide orthodontists with information on bracket behavior due to archwire rotation.

Clinically, this work will indicate whether manufacturer appliances will affect treatment outcomes. In addition, understanding the correct inputs used to achieve tooth motion and their effects on the surrounding tissues will provide clearer understanding of the tooth movement process. Finally, more complete understanding of the tooth movement process will lead to more efficient treatment and improved patient treatment outcomes; a benefit to both clinicians and patients.

The objectives of this paper is to detail the design and development of this novel DIC-based measurement technique used with a modified torque measurement device and assess the level of systematic error associates with the instrumentation within the context of a practical and clinical case-study application. A comparison will be made between the systematic measurement errors to the variability in orthodontic brackets to investigate sources of variability in results. An example test set comparing two styles of bracket will also be discussed to highlight system capability.

2 Description of Orthodontic Bracket Deformation

Pictorial schematics of a classically shaped orthodontic bracket are shown in Fig. 1 which consists of a base, tie wings and an archwire slot in reference to a central incisor tooth. The base is bonded to the tooth using a dental adhesive. The tie wings

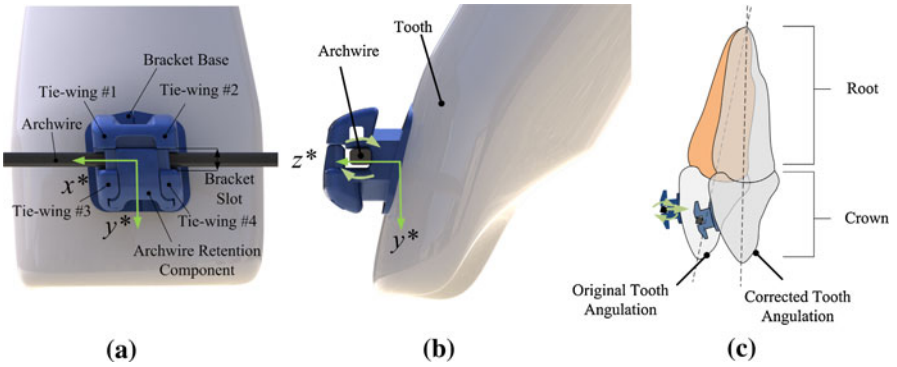

Fig. 1 Self-ligating orthodontic bracket components **a** *Top view* of bracket showing tie wings, archwire and bracket base. **b** *Side view* of bracket showing the angle of the bracket slot (prescription). Archwire rotation occurs about the x^* axis of the bracket coordinate system. **c** Control of tooth angulations using archwire rotation

provide a retentive means to hold an archwire within the bracket slot for this style of bracket using either elastic ligation or stainless steel ligature wires. Alternatively different designs of brackets use self-ligation which include a movable component used for the same purpose without the need for additional ligation [15]. It can be seen in Fig. 1 that for a coordinate system attached to the bracket (x^*, y^*, z^*) the x^* axis is defined as parallel to the archwire, the y^* axis is defined as the direction of lateral motion of the bracket tie wings due to archwire rotation and the z^* axis defines the direction from the base of the orthodontic bracket to the top of the bracket tie wings. Archwire rotation occurs about the x^* axis and the angle of archwire rotation is defined as ϕ. The figure also shows the relative size of the bracket/archwire system compared to the tooth and the complex geometry of the bracket. Change of anterior tooth inclination is achieved by rotating an archwire within an orthodontic bracket slot as shown in Fig. 1c. This figure shows the initial and final tooth angulations. Control over the amount of tooth inclination is necessary in orthodontic treatment in order to maintain post treatment stability and to maintain a healthy alignment of the teeth and is carried out by applying different magnitudes of archwire rotation [1, 16].

3 Design Details of the Orthodontic Torque Simulator

To investigate the interaction of the archwire and bracket a physical simulation of archwire rotation within a bracket slot was developed. The orthodontic torque simulator (OTS) presented in Fig. 2 shows a rendered version of the device in Fig. 2a and a close up digital image of the archwire rotation assembly in Fig. 2b. This custom testing device was required to simulate the clinical situation of archwire rotation and measure the loads applied to the bracket. Additionally, an overhead imaging system was added that collects images of the brackets allowing for digital image correlation (DIC) to be performed on the brackets to identify tie

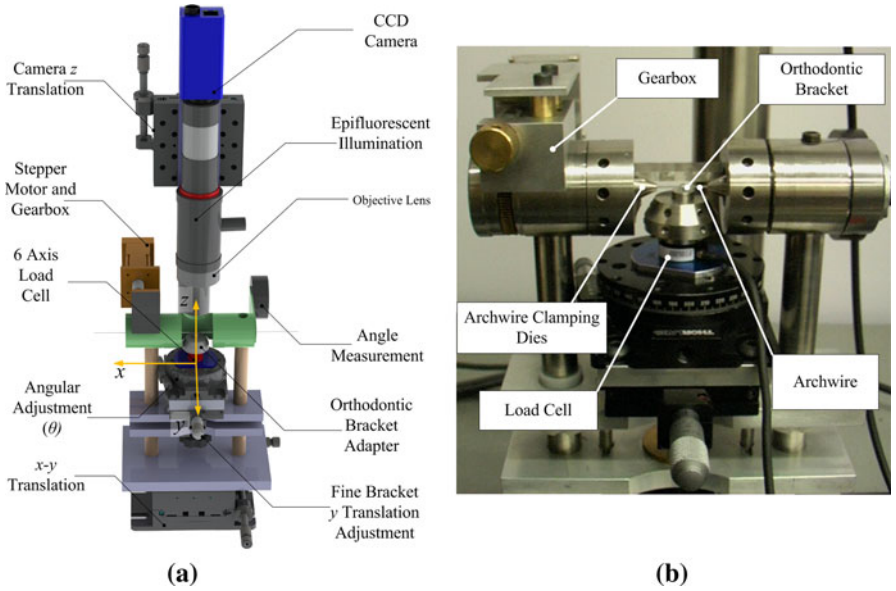

Fig. 2 Device used to measure loads applied to orthodontic brackets and bracket deformation. **a** Rendered image of orthodontic torque simulator. **b** Close-up of the orthodontic torque simulator

wing movement. Figure 2a shows the camera system used to collect images of the orthodontic brackets. Archwire rotation is achieved using a computer controlled stepper motor and gear box. Two dies shown in Fig. 2b are used to clamp the archwire are mechanically locked together by a yoke to provide support to the archwire and even rotation from both sides. Also shown in this figure is the 6-axis load cell which is used to collect force and moment data applied to an orthodontic bracket due to archwire rotation.

3.1 Force and Moment Measurement

The loads applied to the orthodontic brackets were measured using a 6-axis load cell (Nano17 SI-25-0.25, ATI Industrial Automation, Apex, NC, USA) located immediately under the bracket. As shown in Fig. 2b, each bracket for testing was bonded to a standard support cylinder (6 mm diameter stainless steel × 6 mm long) which was held in a support adaptor. The adaptor allowed connection of the bracket\support cylinder to the load cell while allowing adjustment of angular position of the bracket to align with the archwire. The use of this support cylinder and adaptor offsets the measured loads from the applied loads. The specifications and uncertainties for the load cell are shown in Table 1. Data from the load cell was collected using a data acquisition system (DAQ 16-Bit E series NI PCI-6033E; National Instruments, Austin, TX, USA) that had 16 bit input resolution and a maximum sampling rate of 100kS/s. Load cell data was collected at 1,000 Hz and 1,000 samples per channel were recorded for each load cell reading.

Table 1 Specifications of the 6-axis load cell

	F_x	F_y	F_z	T_x	T_y	T_z
Rated full scale loads	25 N	25 N	35 N	250 N mm	250 N mm	250 N mm
Resolution	1/80 N	1/80 N	1/80 N	1/16 N mm	1/16 N mm	1/16 N mm
Measurement uncertainty (percent of full scale load)	1.00 %	1.00 %	1.00 %	1.75 %	1.5 %	1.75 %

3.2 Archwire Rotation Control

Archwire rotation is achieved with a stepper motor (Cool Muscle CM1-C-11L30, Myostat Motion Control Inc., Newmarket, ON, Canada) coupled to a custom design worm and wheel gear box that rotates a yoke that holds the two archwire clamping dies. The clamping dies, gearbox, and archwire are shown in Fig. 2b. The gear system is designed with a 1:96 gear ratio and a 3.75° rotation (1,000 stepper motor counts) represents one revolution of the worm gear. The backlash in the gear system is less than the 0.05° resolution of a inclinometer (model T2-7200-1N; US Digital, Vancouver, WA, USA) which was used for monitoring only. Archwire rotation was defined by the input to the stepper motor which was achieved via serial communication from the control PC and custom software.

3.3 Bracket Position Control

Two translation stages were used to adjust the *x*–*y* position of the entire torque assembly underneath the imaging system (LT01 Translation Stage, Thor Labs, Newton NJ, USA) as shown in Fig. 2a allowing for the bracket to be centered in the camera field of view. A translation stage was also used to control the height (z) of the camera above the orthodontic bracket. Additionally, a translation stage with a micrometer shown in Fig. 2b was used to control the position of the bracket (MT01 Translation Stage, Thor Labs, Newton NJ, USA). This precision translation stage allows for control over the bracket y-position and ensures the archwire can be placed within the bracket slot while minimizing any initial forces or moments. A rotation stage controlling rotation about the z*-axis was used to ensure the bracket slot is also parallel to the archwire (PR01 Rotation Stage, Thor Labs, Newton NJ, USA).

3.4 Bracket Imaging

An imaging system composing of a CCD camera (piA2400 12gm, Basler Vision Technologies, Exton, PA, USA) connected to a long working distance microscope (55-908 MMS R4, Edmund Optics, Barrington, NJ, USA) collected images at 2,448 × 2,050 pixels and 12-bit resolution. The objective lens viewed the top of the bracket, normal to the archwire rotation axis at its nominal working distance of 67 mm. Test specimens are illuminated using epi-illumination (MVO® MMS®

In-Line Attachment 56–244, Edmund Optics, Barrington, NJ, USA) to provide even illumination across the field of view.

3.5 Bracket/Load Cell Force Moment Conversion

The load cell measures forces and moments at the origin of its coordinate system (x, y, z) as defined in Fig. 3. This figure shows a close up render image of the relationship of the load cell to the bracket with the bracket cylinder and mounting adapter. To determine forces and moments applied directly to the bracket by the archwire, a force/moment coordinate transformation is required. The offset of the bracket from the origin of the load cell is measured using a commercial coordinate measurement machine (FaroArm, FARO USA, Lake Mary, FL, USA). The relationship of the two coordinate systems requiring the transformation from the load cell (x, y, z) to the bracket (x^*, y^*, z^*) is illustrated in Fig. 3. The offset of the orthodontic bracket from the load cell comprises of a displacement in the x, y and z-directions as well as a rotation about the z-axis, θ as shown in Fig. 3b.

The transformation of measured forces and torques to bracket forces and torques can be defined as:

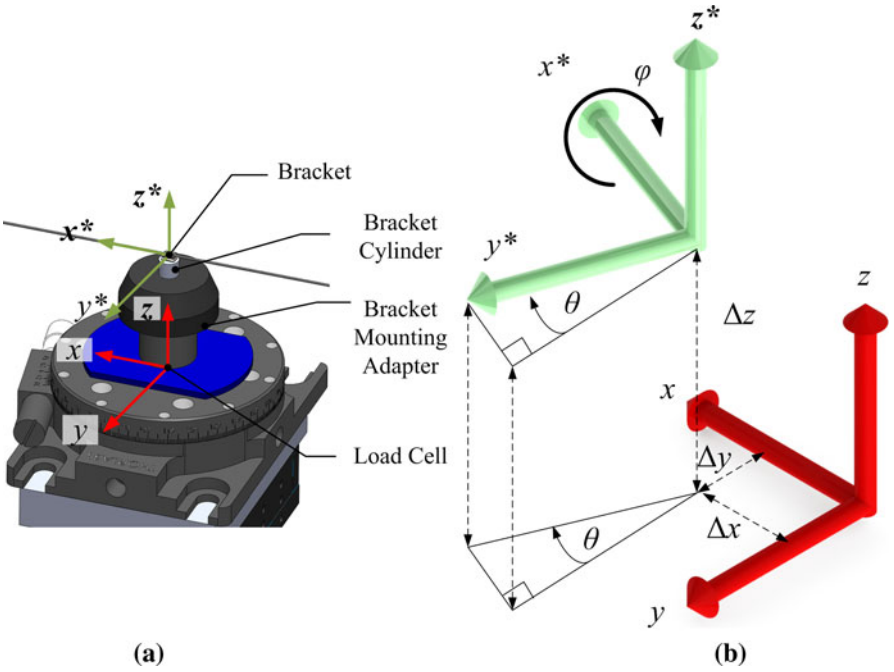

Fig. 3 Load cell and bracket coordinate systems. **a** Offset of orthodontic bracket from load cell. **b** Coordinate system transformation showing displacement, rotation about the z axis and the angle ϕ indicating the direction of archwire rotation

$$F_{bracket} = \begin{pmatrix} m_{xbracket} \\ m_{ybracket} \\ m_{zbracket} \\ f_{xbracket} \\ f_{ybracket} \\ f_{zbracket} \end{pmatrix}$$

where,

$$\begin{aligned} m_{xbracket} &= m_{xLC}\cos\theta - f_{zLC}(\Delta y\cos\theta - \Delta x\sin\theta) + m_{yLC}\sin\theta \\ &\quad + \Delta z\left(f_{yLC}\cos\theta - f_{xLC}\sin\theta\right) \\ m_{ybracket} &= f_{zLC}(\Delta x\cos\theta + \Delta y\sin\theta) + m_{yLC}\cos\theta - m_{xLC}\sin\theta \\ &\quad - \Delta z\left(f_{xLC}\cos\theta + f_{yLC}\sin\theta\right) \\ m_{zbracket} &= m_{zLC} - \Delta x f_{yLC} + \Delta y f_{xLC} \\ f_{xbracket} &= f_{xLC}\cos\theta + f_{yLC}\sin\theta \\ f_{ybracket} &= f_{yLC}\cos\theta - f_{xLC}\sin\theta \\ f_{zbracket} &= f_{zLC} \end{aligned} \tag{1}$$

This relationship converts forces and moments measured at the load cell (i.e. f_{xLC}, the load cell force in the x-direction, m_{xLC} the load cell moment about the x-axis) to forces and moments at the bracket (i.e. $f_{xbracket}$, bracket force in x*-direction, $m_{xbracket}$, bracket moment about the bracket x*-axis). The load cell to bracket transformation equation was determined using a transformation between coordinate frames utilized for robot manipulators [17]. This equation shows that the forces and moments experienced by the bracket depend on the offset of the bracket from the center of the load cell and the rotation of the bracket relative to the load cell.

4 Orthodontic Torque Simulator Experiment

The OTS was controlled using custom designed software (LabWindows/CVI, National Instruments, Austin TX, USA). This program automates the control of the stepper motor, acquisition of data from the load cell and image acquisition. Data recorded from the load cell and current bracket image are displayed on screen to monitor the status of the experiment in real time. Parameters such as the maximum angle of archwire rotation; angle increment; and time between archwire rotations can be controlled using this software. The recording sequence for the OTS is shown in Fig. 4 and highlights the flexibility to run different experiment configurations as well as repeat experiments. The software was designed to allow the system to be used by a variety of researchers with non-specific backgrounds including orthodontic students using the system as part of their graduate research program.

4.1 Overhead Images

An example of an image sequence collected from the OTS of a Damon Q (Ormco Corporation) orthodontic bracket is shown in Fig. 5. The figure shows images

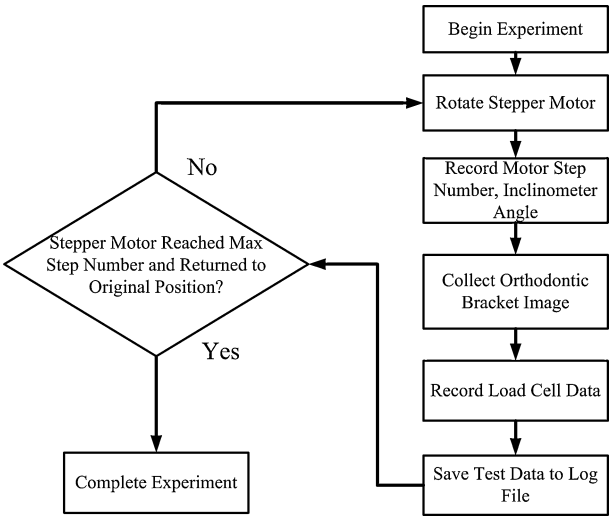

Fig. 4 Flowchart of orthodontic torque simulator operation

collected for every nine degrees of archwire rotation (ϕ) to a maximum angle of 78°. This style of bracket is self-ligating with a door that is closed over the bracket slot to hold the archwire in place. The brackets have been marked using a micro-etcher to provide contrast features on the surface of the bracket. These are needed as part of the DIC analysis which tracks regions of similar contrast to determine displacement. The change in archwire angulations can be seen in each of the successive images. The image sequence also shows the bracket slot opening as a result of archwire rotation.

A profile image of an orthodontic bracket is shown in Fig. 6. Profile images of orthodontic brackets were examined to show the variability in bracket slot sizes [18]. The main image in the figure shows a bracket before an archwire has been rotated in the bracket slot using the OTS. Overlaid on this image is the outline of the same bracket after archwire rotation showing bracket deformation in the x^* and z^* directions defined in Fig. 1. Figure 6 shows that there is localized deformation (notching) where the archwire contacts the bracket slot. Archwire rotation and the forces and moments caused by its rotation can result in both elastic and plastic deformation to the orthodontic bracket tie wings [6]. Deformation of the orthodontic brackets can alter how the bracket behaves due to archwire rotation. An understanding of bracket deformation is necessary to ensure that the desired amount of force is applied to a tooth [7].

4.2 Measured Bracket Force/Moment

In addition to collecting images of orthodontic brackets for successive archwire wire rotation, load cell data is also collected. Load cell data was synchronized with the acquired bracket images allowing for bracket deformation and applied moment to be compared. The measurement that is of most interest to practitioners is the amount of

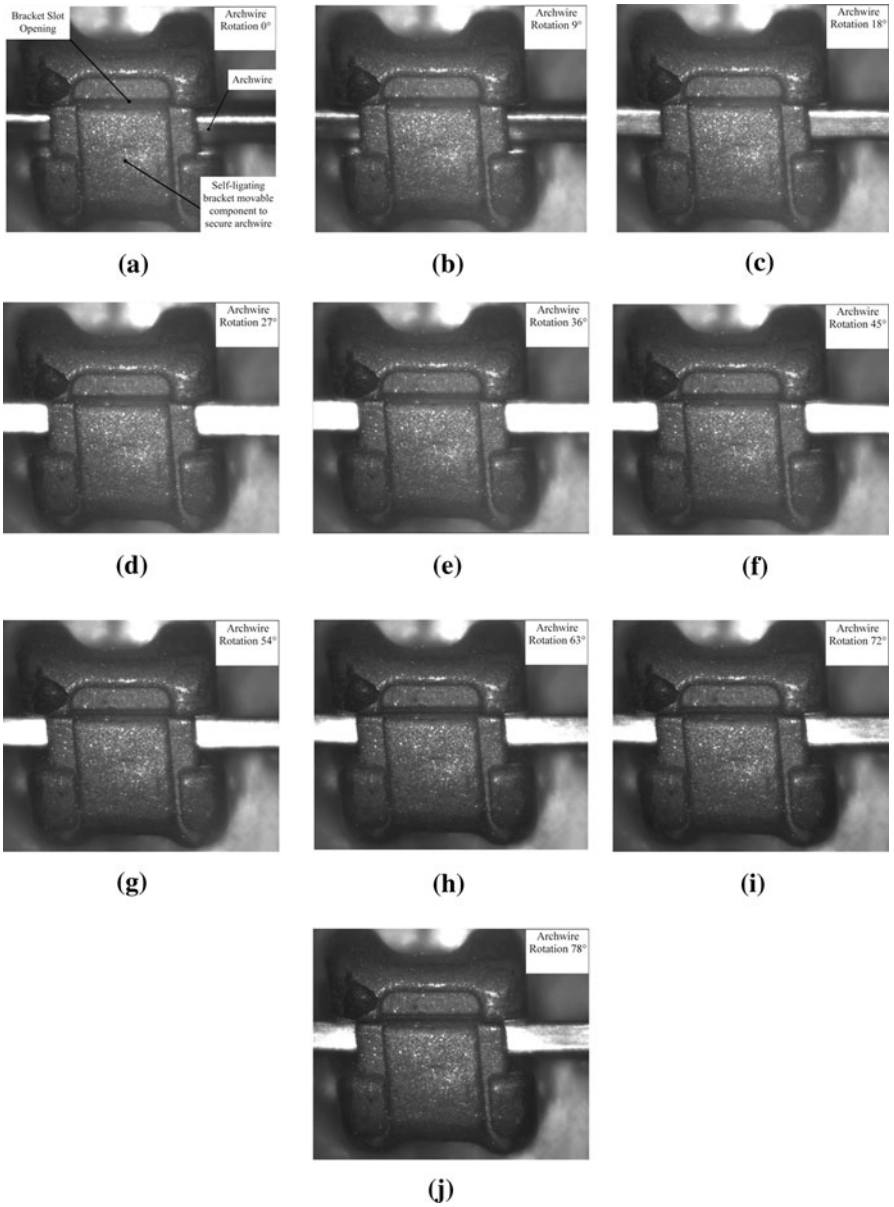

Fig. 5 Deformation of a Damon Q (Ormco Corporation) orthodontic bracket due to archwire rotation. Archwire rotation (ϕ) is shown in 9° increments to a maximum angle of 78°

torque applied to the orthodontic bracket caused by pure archwire rotation ($m_{xbracket}$). Load cell data for a typical 0.019 × 0.025 stainless steel wire (Ormco Corporation) archwire and a self-ligating Damon Q (Ormco Corporation, Orange, California, USA) bracket-archwire combination is shown in Fig. 7 for the

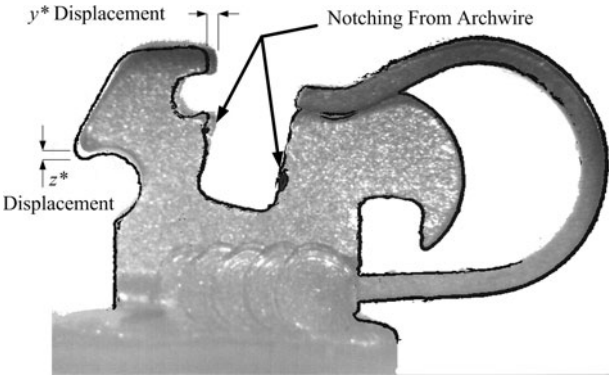

Fig. 6 Profile image of an orthodontic bracket showing the original bracket and the outline of a deformed bracket

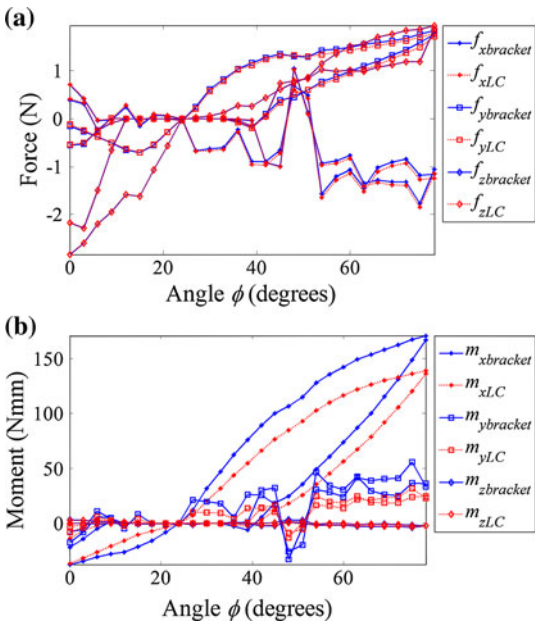

Fig. 7 Load cell transformation showing transformed and measured forces and moments, **a** transformed and measured force (f_x, f_y, f_z). **b** Transformed and measured moments (m_x, m_y, m_z)

determined forces and moments respectively. The need for the bracket/load cell transformation as illustrated in Fig. 3 is required to determine the forces and moments that occur at the bracket instead of at the load cell. The computed transformed forces and moments are also plotted in Fig. 7 for comparison with raw data.

Measurement of a test bracket has been performed to illustrate the force/moment conversion and the propagation of errors that result from this transformation [19]. Measurements of the test bracket offset from the load cell are show in Table 2. Several sources of uncertainty have been identified which will contribute to the

Table 2 Bracket offset from load cell measurements and uncertainty

Measurement	Measured offset	Uncertainty
Δx	−0.4047 mm	±0.018 mm
Δy	0.7673 mm	±0.018 mm
Δz	17.650 mm	±0.018 mm
θ	3°	±0.5°

errors associated with the load cell/bracket transformation, including the load cell force $f_{xLC}, f_{yLC}, f_{zLC}$; load cell moment m_{xLC}, m_{yLC}, m_{zLC}; bracket offset Δx, Δy, Δz and bracket angular offset θ measurement. The uncertainty for the load cell measurements are show in Table 1. Also the FaroARM uncertainty which were used to calculate the bracket/load cell offset listed in Table 2. Error propagation analysis was carried out in order to account for the uncertainty in the load cell/bracket transformation. Equation 2 shows that the load cell/bracket transformation is a function of Δx, Δy, Δz θ, f_{xLC}, f_{yLC}, f_{zLC}, m_{xLC}, m_{yLC}, and m_{zLC}. Equation 2 also shows that the uncertainty in the load cell/bracket transformation is a function of the uncertainty of the offset of the bracket from the load cell (Δx, Δy, Δz, θ) and the uncertainty in the load cell measurement (f_{xLC}, f_{yLC}, f_{zLC}, m_{xLC}, m_{yLC}, m_{zLC}). The individual uncertainties were used to find the total uncertainty in the load cell/bracket transformation.

$$
\begin{aligned}
F_{bracket} &= f\left(\Delta x, \Delta y, \Delta z, \theta, f_{xLC}, f_{yLC}, f_{zLC}, m_{xLC}, m_{yLC}, m_{zLC}\right) \\
u_{F_{bracket}} &= f\left(u_{\Delta x}, u_{\Delta y}, u_{\Delta z}, u_{\theta}, u_{f_{xLC}}, u_{f_{yLC}}, u_{f_{zLC}}, u_{m_{xLC}}, u_{m_{yLC}}, u_{m_{zLC}}\right) \\
\theta_{F_{bracket}} &= \begin{bmatrix} \frac{\partial F_{bracket1}}{\partial x_1} & \cdots & \frac{\partial F_{bracket_n}}{\partial x_n} \\ \vdots & \ddots & \vdots \\ \frac{\partial F_{bracket_m}}{\partial x_1} & \cdots & \frac{\partial F_{bracket_m}}{\partial x_n} \end{bmatrix} \quad n = 1, 2, \ldots 10; \quad m = 1, 2, \ldots 6 \\
u_{F_{bracket_m}} &\left[\sum_{i=1}^{n} \left(\theta_{F_{bracket_{m,i}}} u_{F_{bracket_i}}\right)^2\right]^{1/2} \quad n = 1, 2, \ldots 10; \quad m = 1, 2, \ldots 6
\end{aligned}
\tag{2}
$$

The maximum measurement uncertainty for the measured bracket forces and moments are summarized in Table 3. The uncertainty for the bracket forces and moments was determined by performing an error propagation analysis based on the ASME power test codes (PTC) 19.1 Test Uncertainty test standard discussed in [19]. The uncertainty in the bracket moment $m_{xbracket}$ is indicated by error bars in Fig. 8. The value of $m_{xbracket}$ is the main focus of the OTS measurement system. This value represents the measured moment that has been applied to the bracket due to archwire rotation. The OTS is designed to apply a pure rotation to the orthodontic bracket. In orthodontic pure archwire rotation is known as torque expression [20]. The measured load cell data shows that the magnitude of moment is largest about the x*-axis this can be seen in Fig. 7b. Figure 8 shows changes in applied moment during a loading–unloading cycle, which indicate permanent deformation in the bracket.

Table 3 Maximum bracket force and moment measurement uncertainty

Max $m_{xbracket}$ uncertainty (%)	Max $m_{ybracket}$ uncertainty (%)	Max $m_{zbracket}$ uncertainty (%)	Max $f_{xbracket}$ uncertainty (%)	Max $f_{ybracket}$ uncertainty (%)	Max $f_{zbracket}$ uncertainty (%)
1.44	2.79	2.33	2.18	1.17	1.45

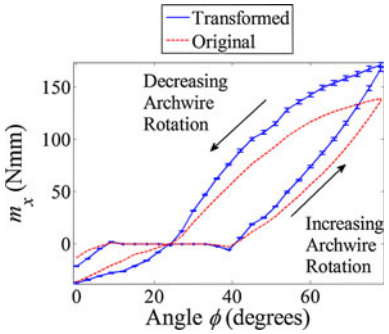

Fig. 8 Load cell transformation showing transformed and measured m_x as well as effect of increasing and decreasing archwire rotation. *Error bars* are shown to demonstrate the uncertainty in the $m_{xbracket}$ measurement

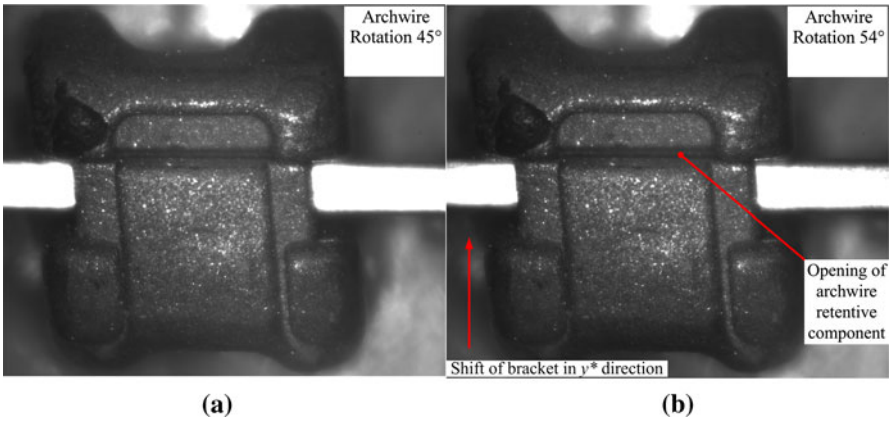

Fig. 9 Engagement of archwire in retentive component of the orthodontic bracket resulting in a change in the measured moment $m_{ybracket}$. **a** Archwire rotation of 45°. **b** Archwire rotation of 54° showing the opening of the archwire retentive component and a displacement in the y^* direction due to archwire rotation

The magnitude of force applied to the bracket as well as $m_{ybracket}$ and $m_{zbracket}$ are small compared to $m_{xbracket}$ as shown in Fig. 7. While $m_{xbracket}$ is the dominate and intentional moment introduced into the system, measured values for the other moments, $m_{ybracket}$ and $m_{zbracket}$ are due to variations in the bracket slot dimensions and the ability to visually align the bracket slot with the archwire. The measured moment $m_{ybracket}$ shows a distinct change at an angles ϕ of 48° and 51°. This change can also be seen in Fig. 9, a detailed set of images about the angle where there is a shift in the position of the bracket. At these angles the corner of the archwire begins

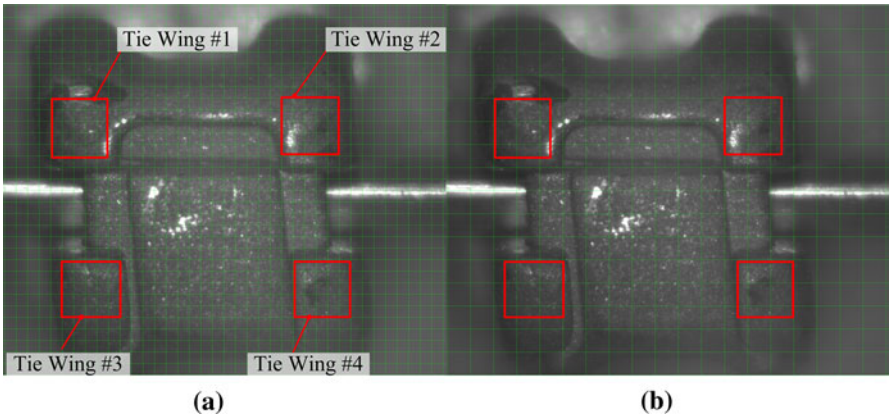

Fig. 10 Bracket images showing image subsets. **a** 64 × 64 pixel subsets. **b** 128 × 128 pixel subsets

to engage the archwire retention component and apply a load to in the z^*-direction of the bracket thus causing a sharp change in the measured moment $m_{ybracket}$ and a sharp change also occurs to the measured force $f_{xbracket}$. This relaxes with increased rotation of the archwire and is believed to be a result of the archwire repositioning within the slot. Additionally, all forces measured by the load cell are small with respect to the applied moment ($m_{xbracket}$). Figure 7b shows that typical forces measured by the load cell range between −2.5 and 1.5 N. The measured moment $m_{xbracket}$ will be used to along with the digital image processing method to better describe the bracket/archwire interaction.

5 Digital Image Correlation of Bracket Images

Images collected using the OTS were processed using a DIC technique in order to ascertain the movement and deformation that occurs to bracket tie wings as an archwire is rotated within a bracket slot. A commercial software package (LaVision GmbH, DaVis 7.2, Göttingen, Germany, 2007) was used to determine the displacement vectors from the set of bracket images that characterize the movement of the bracket. DIC is a full-field measurement technique that measures deformation by comparing the gray intensity levels between successive images [21, 22]. Each digital image is segmented into evenly spaced subsets and an image correlation algorithm is performed for each image subset. The average displacement in each subset is then determined as the displacement vector from the center of the region to the maximum of the correlation function.

Image subsets used in this study ranged in size from 64 × 64 pixels to 256 × 256 pixels. Examples of the subsets used for the DIC algorithm are illustrated in Fig. 10 in comparison to the size and position of the bracket. The field of view for the overhead images is 2,448 × 2,050 pixels or 3.76 × 3.15 mm. Figure 10 also shows the four tie wing box regions that will be used to measure the deformation of the orthodontic brackets. From this figure it can be seen that more

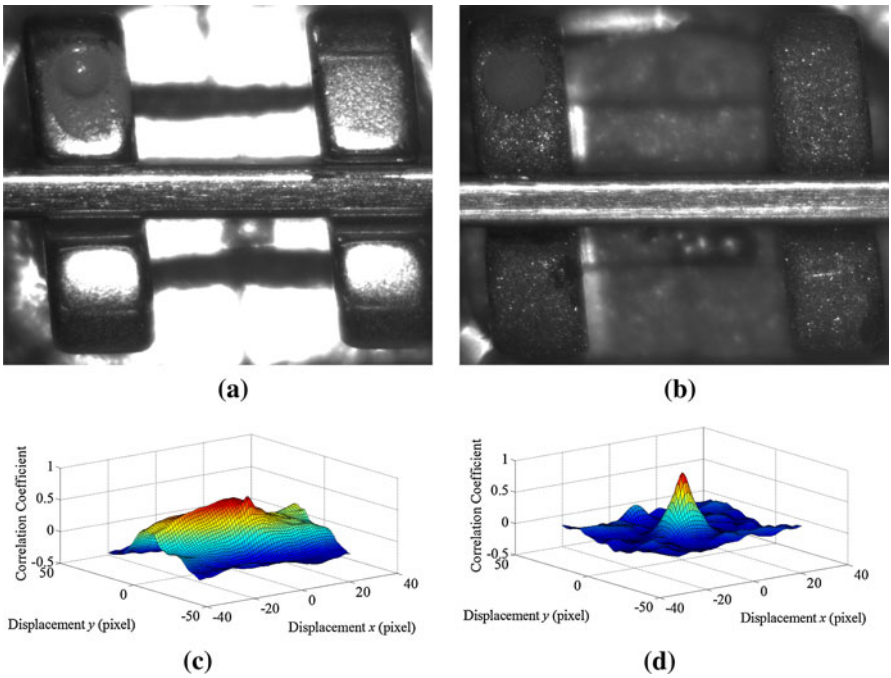

Fig. 11 Preparation of orthodontic brackets. **a** Bracket without micro-etching. **b** Bracket with micro-etching. **c** Correlation peak for bracket without micro-etching. **d** Correlation peak for bracket with micro-etching

pixel subsets are within the tie wing box regions for Fig. 10a, b. The number of subsets will affect the ability to resolve the deformation of the tie wings.

A random speckle pattern was applied to the surface of the orthodontic brackets using a micro-etcher (The Arum Group, Spokane, WA, USA). Micro-etching improved the contrast of the bracket images which has an important effect of the strength and shape of the resultant correlation peak used to determine movement in successive images. A comparison between a bracket with and without speckling is shown in Fig. 11. This figure also shows the corresponding correlation peak for the brackets with and without speckling. From this figure it is evident that a pronounced correlation peak exists for the micro-etched bracket whereas the correlation peak for the bracket without micro-etching is not as distinct. The DIC algorithm will calculate a peak maximum which represents the average displacement within the image subset. A peak detection algorithm is used to locate that maximum within the cross-correlation function and its location within the 2-D function is the magnitude and direction of movement. Examples of the correlation peak generated from the cross correlation algorithm are shown in Fig. 11c, d. The pronounced correlation peak in Fig. 11d shows that a strong correlation can be found between bracket image frame (i) and ($i + 1$) which can be easily be detected by the peck detection section of the DIC system. Conversely, a strong correlation peak does not exist for the bracket image shown in Fig. 11a [23] where similar high intensity light values

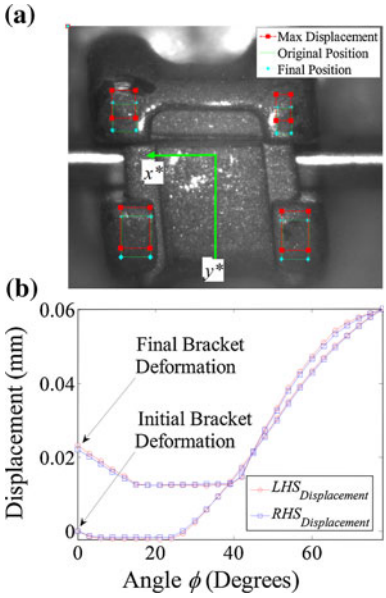

Fig. 12 Tracking of bracket tie wings. **a** Bracket in original position shown by *solid lines*, *square boxes* showing maximum tie wing displacement and *diamonds* showing final tie wing position after applied moment has been removed. **b** Plot of bracket tie wing deformation measured using digital image correlation showing initial and final deformation of the left hand and right hand side of the bracket tie wings

measured by the CCD over a majority of the bracket due to its high reflection broaden the correlation peck. Image data of this type can skew the position of the maximum correlation resulting in a false peak detection that does not represent average movement within the subset. Therefore, all brackets which were examined using the OTS were micro-etched prior to testing. Several processing schemes [21, 22] are available that can be used to improve the accuracy of the DIC algorithm. These algorithms allow for subset window off-set as well as single/multiple pass approaches. The effect of subset window offset and single/multiple pass approaches are discussed below.

Bracket tie wing separation was investigated by tracking a defined region for each tie wing as shown in Fig. 12a. The initial region for each tie wing is shown in the figure as a clean box. The measured displacement in the y^*-direction was determined by averaging the displacement results for the smaller subsets within the defined regions shown in the figure. As the archwire is rotated within the bracket slot relative motion exists between tie wings. Additionally, bulk motion is observed as the entire bracket moves due to the applied loads from archwire rotation and relaxation of the support cylinder within the support adaptor. The maximum movement of the bracket tie wings is shown in Fig. 12a by the position of the boxes with solid squares. Once the archwire reaches the prescribed maximum angle the archwire rotates back to the start position. The final position of the bracket tie wings is shown by the boxes with closed diamonds where it can be seen that the final position of the tie wings is slightly offset from the original position indicating permanent bracket deformation has occurred. The change in average displacement in the y^* direction between the top left and bottom left boxes for Tie Wing #1 and Tie Wing #3 as well as the top right and bottom right brackets of Tie Wing #2 and Tie Wing #4 was used to determine the deformation of the orthodontic brackets this

can be seen in Fig. 12b. This figure shows the difference between the average displacement of Tie Wing #1 and Tie Wing #3 that occurred between these two tie wings in the y^*-direction and is denoted as $LHS_{Displacement}$. Similarly the average displacement of Tie-Wing #2 and Tie Wing #4 is denoted as $RHS_{Displacement}$. Figure 12b shows that there is both hysteresis and permanent deformation occurred to the bracket due to archwire rotation. Figure 12b also shows the result for the displacement of the left and hand right hand tie wing displacement are similar therefore only the $\overline{LHS_{Displacement}}$ will be used for the remainder of this discussion to compare the deformation of brackets of varying geometry. Equation 3 details the calculation of the bracket tie wing displacement in the y^* direction. In this equation denotes the average displacement of the defined regions for Tie Wings 1, 2, 3 and 4 in the y^* direction.

$$\begin{aligned} LHS_{Displacement} &= \overline{Displacement_{TieWing1}} - \overline{Displacement_{TieWing3}} \\ RHS_{Displacement} &= \overline{Displacement_{TieWing2}} - \overline{Displacement_{TieWing4}} \end{aligned} \tag{3}$$

5.1 DIC Method Sources of Error

There are a number of potential sources of error that exist when using a DIC technique. Errors can result from either the measurement devices or due to factors associated with the DIC processing technique [24]. Examples of measurement device errors are the lighting quality, optical lens distortion and test specimen out-of-plane motion. Errors related to the correlation technique are speckle pattern quality, subset size and correlation algorithm used.

The errors associated with the DIC technique were quantified by collecting an image of a bracket from the OTC and then applying artificial displacements to the digital image with a custom program (The MathWorks, Inc., Matlab, Natick, MA, USA). The images were artificially displaced in increments of 1 pixel (1.538 μm) to a maximum displacement of 20 pixels (30.76 μm). This method is commonly used to quantify errors associated with the digital image correlation process [24–26]. A Damon Q (Ormco Corporation, Orange, California, USA) bracket was used to assess the accuracy of the digital image correlation process.

The artificial displacement technique allows for the assessment of the digital image correlation algorithm, image subset size and quality of the speckle pattern. The overhead images collected were processed using a commercial code (LaVision GmbH DaVis 7.4. Gottingen, Germany; 2007). The resolution of the DIC process depends on the size of interrogation window used as shown in Fig. 10, magnification of the image, speckle pattern and lighting. The measurement resolutions for the case investigated are shown in Table 4 [27].

5.1.1 Measurement Errors from Overhead Images

Errors associated with the overhead images were found by calculating the displacement between the tie wings of the orthodontic bracket as shown in Fig. 10. For rigid body translation tests, the displacement between the bracket tie

Table 4 Digital image correlation image displacement vector resolution

Interrogation window size (pixels × pixels)	Vector resolution (pixels)		Orthodontic torque simulator resolution (μm)	
	Min	Max	Min	Max
128 × 128	0.01	0.03	0.01538	0.04614
64 × 64	0.02	0.05	0.03076	0.0769
32 ×	0.05	0.2	0.0769	0.3076
16 × 16	0.1	0.3	0.1538	0.4614

wings should remain constant since deformation has not occurred to the bracket tie wings. A variety of settings were examined for the processing of the overhead images of the orthodontic brackets. The method for determining the optimal processing method was outlined by Crump et al. [28]. The bracket images were processed by varying the subset window size as well as subset windows percent overlap. In addition, the bracket images were also processed using both a single pass and multi-pass DIC approach.

The error associated with each processing method for artificial image displacement is shown in Fig. 13. This figure shows the errors associated with single pass and multi-pass processing as well as the effect of varying subset window size and percent overlap. It is observed that the multi-pass processing approach resulted in lower errors for all window sizes and percent overlap than the single pass approach. It is further shown that the increase in subset window sizes results in improved accuracy of the correlation process. Window cell size is a compromise between spatial and displacement resolution where larger subsets means more data to perform the averaging process.

From Fig. 13 it was found that a good compromise between spatial and displacement resolution for the bracket images is a multi-pass approach with a 64 × 64 window size and a 25 % overlap. As shown in Fig. 10 the bracket tie wings comprise of approximately only 4 sub-windows when using a 128 × 128 pixel window whereas approximately 25 sub-windows are used for the 64 × 64 pixel windows. Therefore, to increase the averaging number used to define average displacement for the tie wing all bracket images collected from the OTS will be processed using a multi-pass approach and a 64 × 64 window size with 25 % overlap. For the current setup of the OTS the measurement resolution is 0.0769 μm (Table 4) since an interrogation window of 64 × 64 was used for the processing of the overhead bracket images. The maximum error found for the multi-pass approach for a window size of 64 × 64 with a 25 % overlap was 0.09 % whereas the maximum error for the single pass approach was 0.23 %.

Using the defined regions shown in Fig. 12, the bracket tie-wing displacement results for 30 Damon Q brackets measured using the OTS is shown in Fig. 14a. Shown in Fig. 14b is the average deformation and computed standard deviations for the same 30 Damon Q brackets tested with the OTS. This figure shows the large variation that exists between brackets. The orthodontic bracket tie wing displacement as the archwire is rotated in the bracket slot is shown in Fig. 14c. This figure

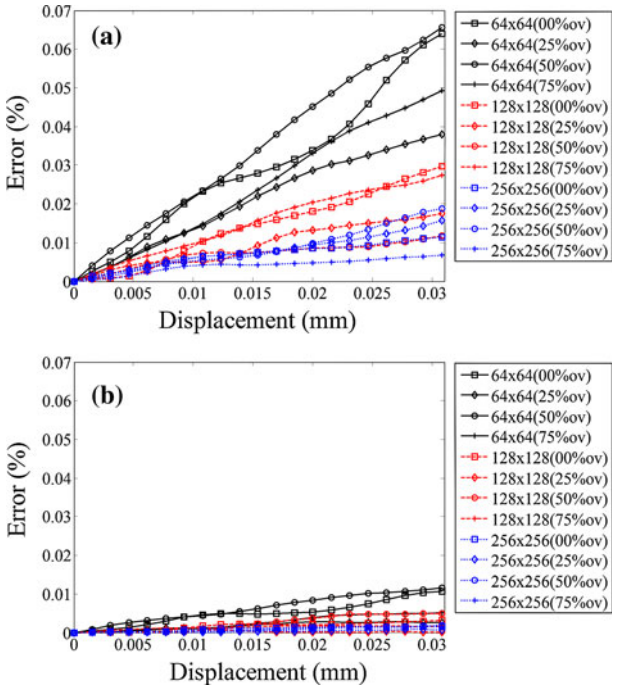

Fig. 13 Effect of window size on overhead images with artificial displacement. **a** Single pass processing. **b** Multi pass processing

shows the displacement of the bracket tie wings for a single Damon Q bracket as well as error bars indicating the uncertainty in the DIC technique. It can be seen that permanent deformation occurred to all the orthodontic brackets since the initial and final tie wing displacement are not the same. The important observation from these figures is that the uncertainty from the optical measurement method is significantly less than the variability found between individual brackets.

6 Orthodontic Bracket Comparison

Two orthodontic brackets of different geometry were compared to exhibit the difference seen for bracket deformation and moment applied due to archwire rotation using the OTS. The brackets were compared to demonstrate the measurement capability of the OTS and to show how varying bracket geometry affects bracket deformation. Both brackets were tested using a 0.4826 $\times$ 0.635 mm (0.019 $\times$ 0.025) stainless steel wire. Both brackets are maxillary right incisor (U1R) with a nominal slot width of 0.5588 mm (0.022). Shown in Fig. 15 are the Damon Q and Speed brackets used for this comparison. From this figure the difference in bracket geometry can be readily seen. Both brackets are self-ligating meaning that no elastic ligature or steel ties are required to hold the archwire in the bracket slot. The two brackets were examined to demonstrate the results produced by the OTS

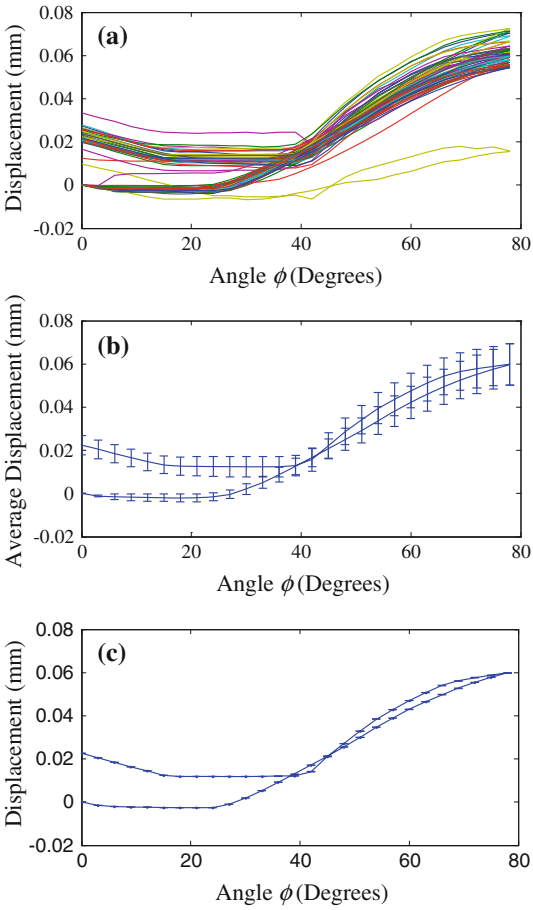

Fig. 14 Orthodontic bracket displacement results. **a** Bracket displacement plots for all 30 brackets. **b** Average of multiple bracket displacement results showing standard deviation for the 30 brackets. **c** Single bracket displacement showing *error bars* resulting from DIC accuracy

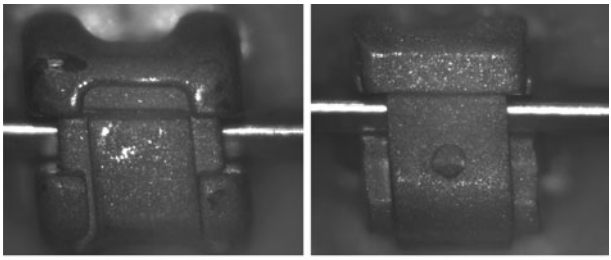

Fig. 15 Comparison of Damon Q (**a**) and Speed (**b**) self-ligating orthodontic brackets

and to show how brackets of different design can be compared using this device. The measured offsets of the brackets from the load cell are summarized in Table 5.

The results from the OTS to compare the Damon Q (Ormco Corporation, Glendora, California, USA) and Speed (Strite Industries, Cambridge, Ontario,

Table 5 Measured bracket offset from load cell

Bracket	Δx (mm)	Δy (mm)	Δz (mm)	θ (degrees)
Damon	−0.6203	0.7399	17.69	3
Speed	−0.4189	0.798	17.65	2

Canada) brackets are shown in Fig. 16 for two individual brackets of this type. Figure 16a compares the deformation of the bracket tie wings 1 and 3 of the two brackets while Fig. 16b shows the measured moment, $m_{xbracket}$ applied to the brackets. From this figure it can be seen that a similar applied moment results in different deformation for the two brackets. Both brackets begin to displace and transmit load at a similar archwire angular position of $\phi \sim 25°$. Moment loading and relative tie wing displacement are non-linear up to maximum archwire rotation. The relative tie wing displacement of the Speed bracket is approximately double that of the Damon Q but transmits $\sim$10 % less moment at maximum archwire rotation. Hysteresis is present for both relative tie wing displacement and transmitted moment for both brackets. Summarized in Table 6 is the maximum measured moment for the two brackets as well as the maximum and final bracket deformation. The final position of the tie wings of the two brackets also shows that the Speed bracket exhibited greater plastic deformation than the Damon Q bracket. Figure 16 and Table 6 demonstrate that the maximum deformation of the Damon Q bracket is 3.2 times less than the Speed bracket. Additionally, the error bars associated with the optical measurement and error from the load cell transformation are shown with the results in Fig. 16. These two figures show that the measurement uncertainty from the OTS is small compared to the difference seen in the deformation and measured moment of the two brackets.

7 Discussion

Several studies have examined the effect of archwire rotation on orthodontic brackets [4–7, 9–11]. The major focus has been on measurement of the moment applied to the orthodontic bracket by the rotating archwire. Several of these studies have made reference to bracket deformation but the deformation was not quantified [4, 5, 7].

The OTS presented here is capable of measuring the final deformation of orthodontic brackets due to archwire rotation. In addition, this device allows for measurement of the deformation that occurs due to successive increases in archwire angle. Force and moment data is also recorded for each archwire rotation. As a result the presented OTS is capable of measuring both the elastic and plastic bracket deformation. Both the elastic and plastic deformation of the orthodontic brackets should be understood since both deformations result in energy lost to the deformation of the orthodontic bracket rather than causing tooth movement. Additionally, the OTS is capable of measuring the forces and moments applied to the orthodontic bracket using a 6-axis load cell. Since load cell measurement and images of the bracket are taken simultaneously The OTS data can be used to match these two measurements.

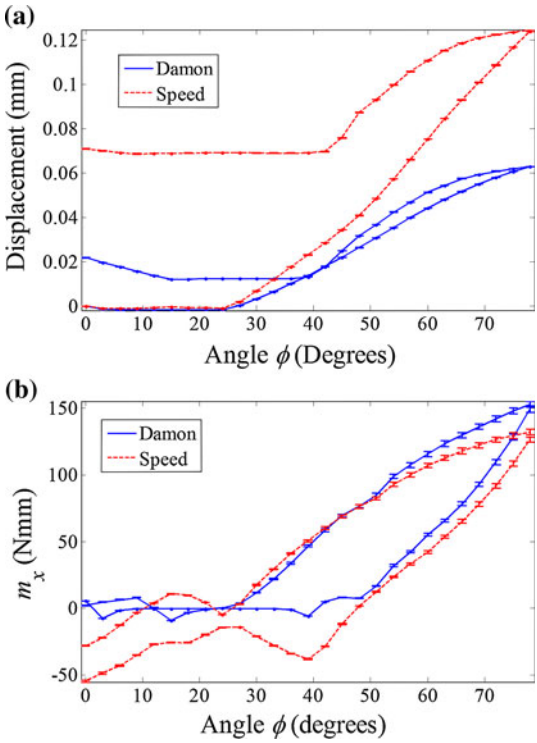

Fig. 16 Comparison of Damon Q and Speed orthodontic brackets. **a** Deformation results. **b** Measured applied moment

Table 6 Comparison of orthodontic bracket deformation results

Bracket	Maximum measured moment m_x (N mm)	Maximum deformation (mm)	Final deformation (mm)
Damon Q	152.7	0.0628	0.0217
Speed	132.0	0.1246	0.0709

Two orthodontic brackets were compared to demonstrate how results from the OTS can be used to compare brackets of varying make and geometry. This comparison shows that the maximum and final deformation of the Damon Q brackets is less than the Speed bracket for the same amount of archwire rotation. As well, 30 brackets of the design Damon Q were analyzed to show that the variability in the orthodontic brackets is much greater than the measurement uncertainty of this device.

8 Conclusions

It was demonstrated that the OTS was been designed to measure the forces and moments applied to orthodontic brackets. The maximum bracket force and moment

measurement uncertainty are significantly less than both the range of movement and moments expected and the observed variability within the bracket design. This device is also capable of measuring the displacement of the orthodontic bracket tie-wings due to archwire rotation within 0.09 % error. Two sample orthodontic brackets were compared to demonstrate how this device can be used to compare brackets of varying geometry. From this comparison presented it was found that maximum deformation of the Damon Q bracket is 3.2 times less than the Speed bracket for similar magnitudes of applied moment. An understanding of the elastic and plastic deformation that occurs to brackets is critical to clinicians since brackets are selected for treatment based on the advertised prescription the particular bracket provides to apply moments to tooth crown. Bracket deformations can alter the geometry of the bracket slot which can affect the efficiency of the treatment. Knowledge of bracket deformation will allow clinicians to select brackets based on the expected deformation that will occur or to adjust the treatment regime to compensate for bracket deformation.

References

1. Proffit, W. R., Fields, H. W., & Sarver, D. M. (2007). *Contemporary orthodontics*. St Louis, Mo: Elsevier.
2. Beckwith, F. R., Ackerman, R. J, Jr, Cobb, C. M., & Tira, D. E. (1999). An evaluation of factors affecting duration of orthodontic treatment. *American Journal of Orthodontics and Dentofacial Orthopedics, 115*, 439–447.
3. Nanda, R., & Kuhlberg, A. (1997). Principles of biomechanics. In R. Nanda (Ed.), *Biomechanics in clinical orthodontics* (pp. 1–20). Philadelphia, PA: Saunders.
4. Gmyrek, H., Bourauel, C., Richter, G., & Harzer, W. (2002). Torque capacity of metal and plastic brackets with reference to materials, application, technology and biomechanics. *Journal of Orofacial Orthopedics, 63*, 113–128.
5. Sadat-Khonsari, R., Moshtaghy, A., Schlegel, V., Kahl-Nieke, B., Möller, M., & Bauss, O. (2004). Torque deformation characteristics of plastic brackets: A comparative study. *Journal of Orofacial Orthopedics, 65*, 26–33.
6. Kapur, R., Sinha, P. K., & Nanda, R. S. (1999). Comparison of load transmission and bracket deformation between titanium and stainless steel brackets. *American Journal of Orthodontics and Dentofacial Orthopedics, 116*, 275–278.
7. Flores, D. A., Choi, L. K., Caruso, J. M., Tomlinson, J. L., Scott, G. E., & Jeiroudi, M. T. (1994). Deformation of metal brackets: A comparative study. *Angle Orthodontist, 64*, 283–290.
8. Feldner, J. C., Sarkar, N. K., Sheridan, J. J., & Lancaster, D. M. (1994). In vitro torque-deformation characteristics of orthodontic polycarbonate brackets. *American Journal of Orthodontics and Dentofacial Orthopedics, 106*, 265–272.
9. Badawi, H. M., Toogood, R. W., Carey, J. P. R., Heo, G., & Major, P. W. (2008). Torque expression of self-ligating brackets. *American Journal of Orthodontics and Dentofacial Orthopedics, 133*, 721–728.
10. Meling, T. R., Odegaard, J., & Meling, E. O. (1997). On mechanical properties of square and rectangular stainless steel wires tested in torsion. *American Journal of Orthodontics and Dentofacial Orthopedics, 111*, 310–320.
11. Odegaard, J., Meling, T., & Meling, E. (1994). An evaluation of the torsional moments developed in orthodontic applications. An in vitro study. *American Journal of Orthodontics and Dentofacial Orthopedics, 105*, 392–400.
12. Lacoursiere, R., Nobes, D., Homeniuk, D., Carey, J. P., Badawi, H., & Major, P. W. (2010). Measurement of orthodontic bracket tie wing elastic and plastic deformation by arch wire torque

expression utilizing an optical image correlation technique. *Journal of Dental Biomechanics, 2010*(Article ID 397037).
13. Major, T. W., Carey, J. P., Nobes, D. S., Heo, G., Melenka, G. W., & Major, P. W. (2011). An investigation into the mechanical characteristics of select self-ligated brackets at a series of clinically relevant maximum torquing angles: Loading and unloading curves and bracket deformation. *European Journal of Orthodontics*. doi:10.1093/ejo/cjr076.
14. Melenka, G. W., Lacoursiere, R. A., Carey, J. P., Nobes, D. S., Heo, G., & Major, P. W. (2011). Comparison of deformation and torque expression of the orthos and orthos Ti bracket systems. *European Journal of Orthodontics*. doi:10.1093/ejo/cjr120.
15. Brantley, W. A., & Eliades, T. (2001). Orthodontic brackets. In W. A. Brantley & T. Eliades (Eds.), *Orthodontic materials: scientific and clinical aspects* (pp. 144–147,165). New York: Thieme.
16. Jayade, V., Annigeri, S., Jayade, C., & Thawani, P. (2007). Biomechanics of torque from twisted rectangular archwires. *Angle Orthodontist, 77*, 214–220.
17. Paul, R. P. (1981). *Robot manipulators: Mathematics, programming, and control: the computer control of robot manipulators*. Cambridge, Mass: MIT Press.
18. Major, T. W., Carey, J. P., Nobes, D. S., & Major, P. W. (2010). Orthodontic bracket manufacturing tolerances and dimensional differences between select self-ligating brackets. *Journal of Dental Biomechanics, 2010*, 781321.
19. Figliola, R. S. (2011). Uncertainty analysis. In A. Melhorn (Ed.), *Theory and design for mechanical measurements* (5th ed., p. 161). Hoboken, NJ: Wiley.
20. Wagner, J. A., & Nikolai, R. J. (1985). Stiffness of incisor segments of edgewise arches in torsion and bending. *Angle Orthodontist, 55*, 37–50.
21. Sutton, M. A., Orteu, J. J., & Schreier, H. W. (2009). *Image correlation for shape, motion and deformation measurements: Basic concepts, theory and applications*. New York, NY: Springer.
22. Pan, B., Qian, K., Xie, H., & Asundi, A. (2009). Two-dimensional digital image correlation for in-plane displacement and strain measurement: A review. *Measurement Science and Technology, 20*, art. no. 062001.
23. Raffel, M., Willert, C., Wereley, S., & Kompenhans, J. (2007). Mathematical background of statistical PIV evaluation. In *Particle image velocimetry: A practical guide* (2nd ed., p. 79). New York: Springer.
24. Haddadi, H., & Belhabib, S. (2008). Use of rigid-body motion for the investigation and estimation of the measurement errors related to digital image correlation technique. *Optics and Lasers in Engineering, 46*, 185–196.
25. Chu, T. C., Ranson, W. F., & Sutton, M. A. (1985). Applications of digital-image-correlation techniques to experimental mechanics. *Experimental Mechanics, 25*, 232–244.
26. Hild, F., & Roux, S. (2006). Digital image correlation: From displacement measurement to identification of elastic properties—A review. *Strain, 42*, 69–80.
27. LaVision GmbH. Product-manual for DaVis 7.2 StrainMaster 2D Item-Number(s): 1105021.
28. Crump, D. A., Dulieu-Barton, J. M., & Savage, J. (2010). Design and commission of an experimental test rig to apply a full-scale pressure load on composite sandwich panels representative of an aircraft secondary structure. *Measurement Science and Technology, 21*, art. no. 015108.